Detection of Land Cover Change in Mie Prefecture Using Sentinel-2 Time Series

Ohashi H.[1] and Matsuoka M.[1*]

[1]Graduate School of Engineering, Mie University, 1577, Kurima-machiya, Tsu, Mie 514-8507, Japan

*matsuoka@info.mie-u.ac.jp

Abstract: *Land cover is important information for understanding the natural environment and for considering national land use planning. Automatic detection of land cover change from satellite images will improve the efficiency of land cover information utilization. The objective is to detect land cover change in Mie Prefecture using the Sentinel-2 time series. Multispectral Instrument (MSI) onboard Sentinel-2 was used because it has a higher spatial (10 m) and temporal (5 days) resolutions than other medium spatial resolution satellites. Since optical sensors are affected by clouds, accurate cloud discrimination is required for accurate detection of land cover change. To improve the accuracy of cloud detection, a cloud mask was created in this study using the Advanced Himawari Imager (AHI) onboard the geostationary Himawari satellite. The cloud mask generated from time series AHI data was applied to the pre-processing step of change detection by the Sentinel-2 MSI. The false positive error of land cover change was greatly reduced by using the AHI generated cloud mask. Since the cloud mask could not completely remove clouds, the remaining clouds were detected based on the smoothness of the reflectance time series for each pixel. To account for the seasonal change of vegetation, land cover changes are detected by comparing time-series data from two consecutive years. In addition, the influence of remaining thin or small clouds and those shadows were considered in change detection by taking the median of time series samples. Land cover change was detected by applying the threshold to the calculated degree of change. Accuracy was evaluated using validation data generated by visual discrimination of Sentinel-2 images. Overall accuracy was 0.34 in case of the detection using band 5. False positives were frequent at the agricultural fields or cloud shadows. False negative could be modified by combining with other bands. If false positives due to vegetation changes can be excluded, false positives will be greatly reduced and the threshold can be relaxed, which will greatly increase the overall accuracy. In addition to the location of the change, we will evaluate the timing of the change in the next step.*

Keywords: Cloud screening, Himawari AHI, Land cover change, Sentinel-2 MSI, Time series analysis

Introduction

Land cover change is important information for understanding the natural environment and for discussing national land use planning. Recently, Satellite images was used to assess the disaster caused by the Noto Peninsula Earthquake of 2024 (Ministry of Land, Infrastructure, Transport and Tourism 2024). The detection of land cover change from satellite images will improve the efficiency of land cover information utilization. In addition, the number of satellites has been increasing at an accelerating rate in recent years, due in part to the

increase in the number of satellite launches by various companies. However, optical sensors are affected by clouds, hence accurate detection of land cover change requires highly accurate cloud discrimination.

The Landsat series of satellites has been used in various land cover applications because they have long history and relatively short temporal resolution of 16 days. In recent years, the Sentinel-2 has been also used because it has approximately 10 years of operation since 2015, with higher spatial and temporal resolutions than those of Landsat. Therefore, Sentinel-2 is capable of detecting more detailed changes and early changes. Sentinel-2 also has more bands and can detect different types of changes. We used Sentinel-2 time series even though the available temporal coverage is shorter than that of Landsat because our target area (Mie Prefecture, Japan) has complex land cover with small patches.

Problem statement

Coluzzi et al. (2018) evaluated the Sentinel-2 Level 1C (L1C) cloud mask. The results showed that the L1C cloud mask generally underestimated the presence of clouds (average Omission Error, OE, 37.4%); this error increased (OE > 50％) for imagery containing opaque clouds with a large transitional zone (between the cloud core and clear areas) and cirrus clouds, fragmentation emerged as a major source of omission errors. An example of a Sentinel-2 cloud mask is shown in Figure 1. Larger clouds have been removed, but there remain many clouds that have not been removed.

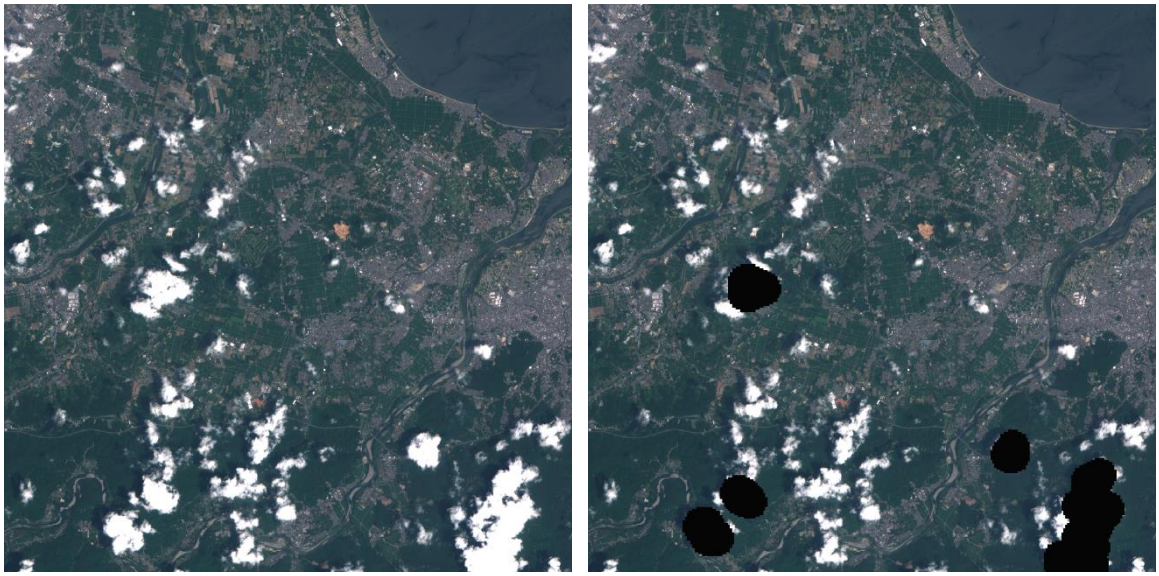

(a) Color image of Sentinel-2 (b) Cloud mask

Figure 1: Example Of Sentinel-2 Cloud Mask

The presence of residual clouds frequently results in erroneous positive indications with regard to land cover change detection, whereby locations that have remained unaltered are identified as having undergone transformation. Therefore, cloud masks must be created more accurately to reduce false positives. The AHI onboard the geostationary Himawari satellite is capable of making observations at intervals as short as 2.5 minutes, which renders it an optimal instrument for cloud detection.

Objective

The objective is to detect land cover change in Mie Prefecture using the Sentinel-2 time series. For this purpose, a cloud mask is created by Himawari/AHI and combined with the Sentinel-2 cloud mask to improve the accuracy of change detection.

Literature survey

Zhu and Woodcock (2014) developed a new algorithm for Continuous Change Detection and Classification (CCDC) of land cover using Landsat time series. They used all bands of Landsat to create a time series model composed of seasonality, trends, and breaks to estimate surface reflectance. A pixel is labeled as changed when the difference in reflectance between observed and model-predicted images exceeds a threshold in three consecutive scenes. The accuracy assessment showed that CCDC results were accurate for detecting land surface change, with producer's accuracy of 98% and user's accuracies of 86% in the spatial domain and accuracy of 80% in the temporal domain. Chai and Li (2023) proposed a method called the Ensemble of Bidirectional Time Series Analysis (EBTSA) method, which combines bidirectional CCDC and Chow Test. This method improves the robustness against data scarcity in earlier times and reduce break detection errors and refine classification results. Overall accuracy was 8.9 percentage points higher than CCDC.

Verbesselt et al. (2010) proposed Breaks For Additive Seasonal and Trend (BFAST), an integrated method for decomposing time series into trend, seasonal, and remainder components and detecting changes. They tested BFAST by simulating 16-day NDVI time series with varying amounts of seasonal amplitude and noise, containing abrupt disturbances (e.g. fires) and long-term phenological changes. This revealed that the method is able to detect the timing of phenological changes within time series while accounting for abrupt disturbances and noise. Verbesselt et al. (2012) applied BFAST to propose a multi-

purpose time-series-based disturbance detection approach that identifies and models stable historical variation to enable change detection within newly acquired data. Simulations of time series of vegetation greenness data from satellite data showed that it is robust to seasonality and noise, yet can be detected in near real time.

Wright et al. (2024) proposed CloudS2Mask, a new open-source Python deep learning library for accurate and efficient detection of clouds and cloud shadows in Sentinel-2 data. CloudS2Mask is trained on multiple large global datasets including CloudSEN12, KappaSet, Sentinel-2 Cloud Mask Catalogue, Sentinel-2 reference cloud masks generated by an active learning method and a custom CloudS2Mask dataset. CloudS2Mask achieved Balanced Overall Accuracy values of 0.930 and 0.963 in the "all types of clouds" and "without thin clouds" experiments, respectively.

Methodology

a. Data

The study area is in central Mie Prefecture and covers an area of 316.84 km^2 with a length and width of 17.8 km. We used Sentinel-2A and 2B (level 1C) data with low cloud cover observed from January 1, 2019 to December 31, 2022. Figure 2 is an image of the study area. We also used Japan Area data from the Advanced Himawari Imager (AHI) onboard the Himawari satellite at the closest observation time with Sentinel-2. Detailed specifications for Sentinel-2 are shown in Table 1. Table 2 shows the spectral range and resolution for each band (Sentinel Online 2024). The four bands were selected one by one from visible, visible and near infrared (VNIR), near infrared (NIR), and shortwave infrared (SWIR). Sentinel-2 data were downloaded via Copernicus Open Access Hub (2024), considering the geographic locations, season, and cloud coverage.

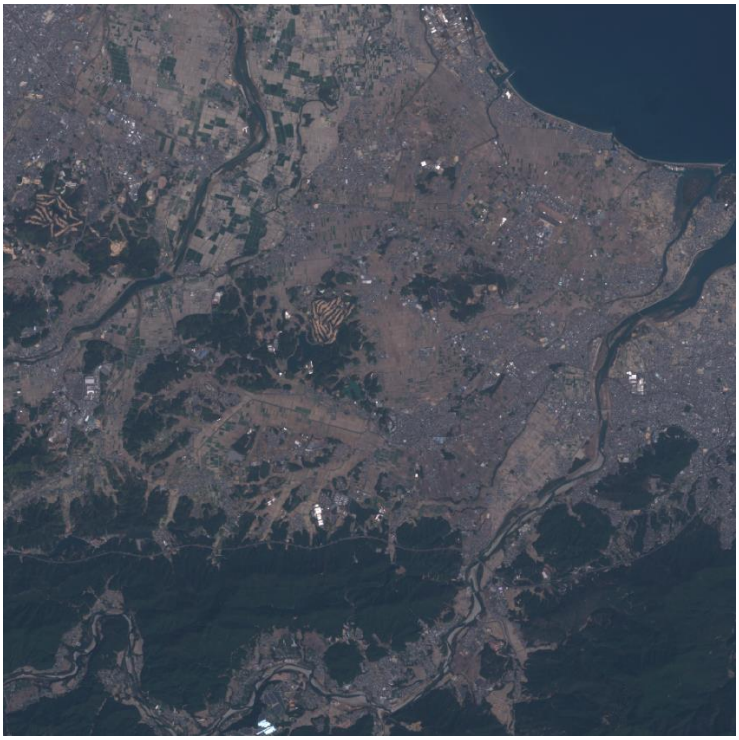

Figure 2: Study Area.

Table 1: Sentinel-2 Specifications.

	Sentinel-2A	**Sentinel-2B**
Operation organization	European Space Agency, European Commission	
Start of operation	June 23, 2015	March 7, 2017
Sensor	Multispectral Instrument (MSI)	

Table 2: Spectral Bands Used in This Study.

Band	**Sentinel-2A**		**Sentinel-2B**		
	Central Wavelength	**Width**	**Central Wavelength**	**width**	**Resolution**
Band 4	664.6 nm	31 nm	664.9 nm	31 nm	10 m
Band 5	704.1 nm	15 nm	703.8 nm	16 nm	20 m
Band 8	832.8 nm	106 nm	832.9 nm	106 nm	10 m
Band 11	1613.7 nm	91 nm	1610.4 nm	94 nm	20 m

b. Preprocessing

The processing version of Sentinel-2 was updated on January 25, 2021 (SentiWiki 2024). The offset value was set in the digital number of the pixel, and it caused the large difference

between old and new data. Accordingly, the following conversion was applied to the existing data set in order to adjust the value range of the data.

$$L1C_{TOAi} = L1C'_{TOAi} + RADIO\_ADD\_OFFSETi$$

where $L1C_{TOAi}$ is the adjusted digital number of pixels, $L1C'_{TOAi}$ is the original digital number in the old version of the data, and RADIO_ADD_OFFSETi is the added offset.

c. Outline

A flowchart of the entire process is shown in Figure 3.

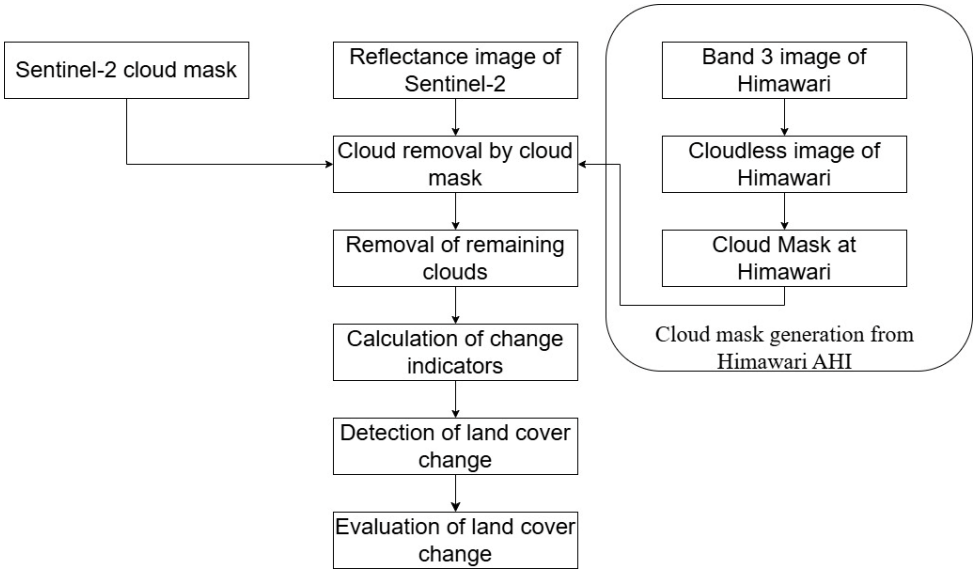

Figure 3: Flowchart Of Image Analysis

d. Cloud Mask Generation from Himawari AHI

To generate the cloud mask for the Sentinel-2 MSI from Himawari AHI observed at almost the same time, the cloud-free image for AHI was generated for each month using all the data observed in the same month for four years (about 120 images). Cloud-free reflectance was calculated by averaging the data of a certain number of the lower reflectance data for each pixel. The number of data used to calculate the averages was adjusted monthly as the results were viewed. In this process, precise geometric correction was applied to correct Himawari's position error (Matsuoka et al. 2015). The observed Himawari image and the created cloud-free image were compared pixel by pixel, and the pixel was determined to be clouds if the following condition was satisfied.

$$O_{x,y} - C_{x,y} > T_{x,y}$$

where $O_{x,y}$, $C_{x,y}$, and $T_{x,y}$ are the reflectance of observed data, the reflectance of cloud-free data, and the cloud discrimination threshold at pixel position (x,y), respectively.

Sentinel-2 has a narrow observation swath, so clouds are projected just below its position. However, for Himawari in geostationary orbit, the projected position changes depending on the height of the clouds (Figure 4). Therefore, we first estimated the cloud height using the following steps.

i) Ortho-rectification Himawari data with different cloud heights (Matsuoka and Yoshioka 2023).

ii) Calculation of the image correlation with Sentinel-2.

iii) The height with the highest correlation will be the cloud height.

This process was applied to all cloud pixels to estimate the horizontal position and height of the clouds. The cloud mask was then converted from the Normalized Geostationary Projection to the Universal Transverse Mercator (UTM) projection to match the Sentinel-2 image, taking into account the cloud positions. The spatial resolution of the cloud mask was set to 500 m according to Himawari's band 3.

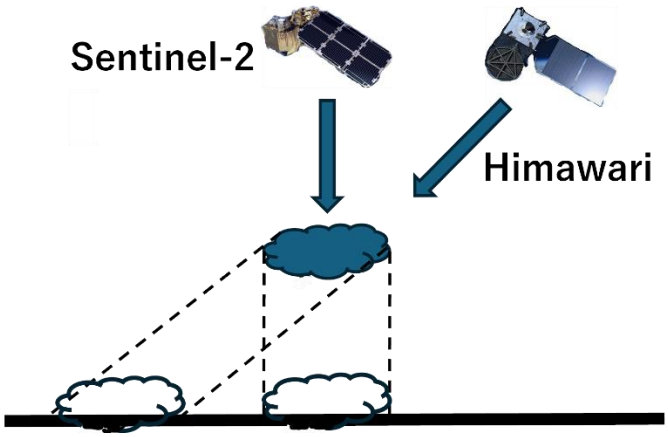

Figure 4: Cloud Displacement By Different Satellite Orbits.

e. Removal of Remaining Clouds

Remaining thin or small clouds were removed based on the stability of time series data. The cloud flag was assigned to pixels that met the following conditions.

$$O_{x,y,t} > M_{x,y} + 3 \times S_{x,y}$$

where $O_{x,y,t}$ is the reflectance at pixel position (x,y) observed at time t, $M_{x,y}$, and $S_{x,y}$ are the mean and standard deviation derived from all time series at pixel position (x,y), respectively. Removing pixels with cloud flags as they are may exclude pixels with land cover changes. Therefore, pixels 15 days before and after the pixel with a cloud flag were checked and removed if there were no other cloud flags.

f. Calculation of Change Indicators

Change is detected by comparing time series data for two consecutive years. There might be clouds or cloud shadows that were not completely removed during the cloud removal process. Therefore, the change indicators were calculated using the median value from the data of the previous and following periods. The calculated change indicators are compared to a threshold value to detect change.

$$d_{before} = \{a_{1-L}, a_{1-L+1}, \dots, a_{N+L}\}$$
$$d_{after} = \{b_{1-L}, b_{1-L+1}, \dots, b_{N+L}\}$$
$$I_t = median(|a_{t-L} - b_{t-L}|, |a_{t-L} - b_{t-L+1}|, \dots, |a_{t+L} - b_{t+L-1}|, |a_{t+L} - b_{t+L}|)$$
$$D_{change} = \{I_1, I_2, \dots, I_N\}$$

where d_{before} and d_{after} are the reflectance time series data for two consecutive years at a pixel. Here, data for period L were added at the beginning and the end of the time series for sliding temporal window processing. I_t is the index of change at time t, the median value selected from the absolute difference calculated for combinations of non-cloudy data, and D_{change} is time series of I.

g. Detection of land cover change

The change indicator for no change is close to zero for any land cover, so a fixed value threshold was used to detect change. This threshold was determined manually for each band with reference to the value of the evaluation index. The results of the four bands were combined so that a change was assumed to have occurred when a change was detected in any one of the bands.

h. Evaluation of land cover change

Accuracy was evaluated using validation data generated by manual detection of changed area using Sentinel-2 images. All of this validation data was generated using QGIS (2024). Precision, Recall, and F-measure were used as evaluation indices. The formulas for each of the evaluation indicators are as follows. Also, band 4 and 8 have a spatial resolution of 10 m, but band 5 and 11 have a spatial resolution of 20 m, so band 4 and 8 were combined for 20 m.

$$Precision = \frac{TP}{TP + FP}$$

$$Recall = \frac{TP}{TP + FN}$$

$$F_{measure} = \frac{2 \times Recall \times Precision}{Recall + Precision}$$

where TP, FP, and FN are the number of pixel in the confusion matrix shown in Table 3.

Table 3: Confusion Matrix

		Detection Result	
		Change	No change
Reference Data	Change	TP	TN
	No change	FP	FN

The accuracy was changed by the sample number of unchanged pixels, therefore we evaluated the accuracy in the following two typical cases:
(1) the same number of unchanged pixels as changed pixels were randomly selected, and
(2) the whole pixel other than changed pixel were used as unchanged pixels.
Accuracy evaluation was calculated based on the results detected in each of the four bands and the combined results.

Results and Discussion

a. Cloud removal results

Figure 5 shows an example of the removal of clouds. The Himawari-based mask could remove cloud accurately, by combining with original cloud mask of Sentinel-2. It can be seen that the clouds are well masked.

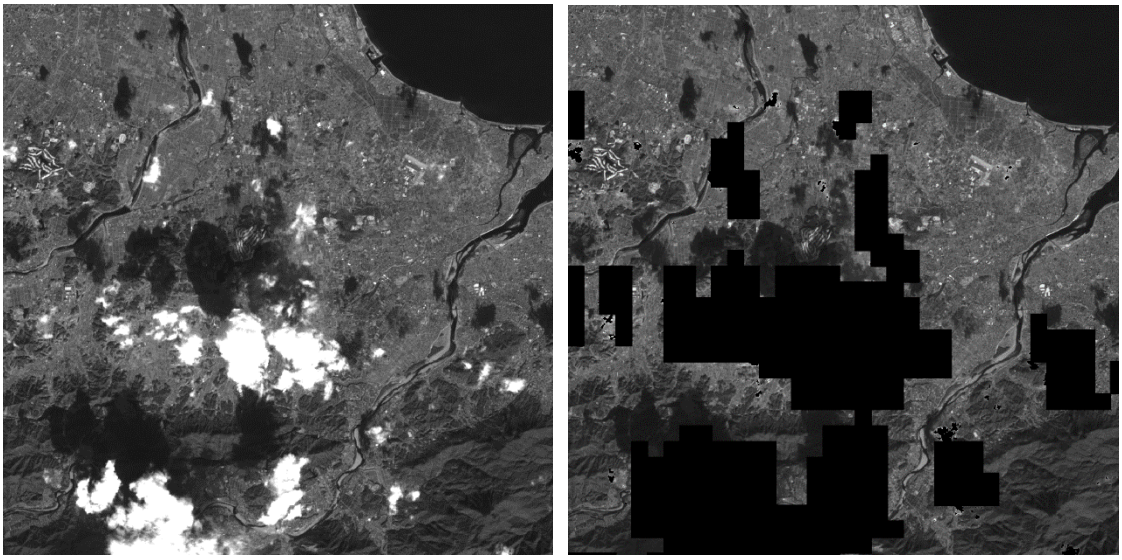

(a) band 5 reflectance image (b) after cloud removal

Figure 5: An Example Of Cloud Removal.

A comparison of time series before and after cloud removal is shown in Figure 6. Both thick and thin clouds can be seen in the time series before cloud removal in mid 2021 and early 2022, respectively. However, we can see that both types of clouds can be removed.

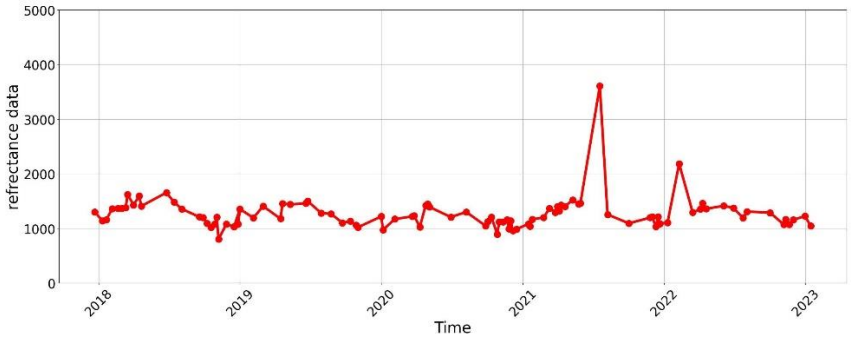

(a) Before cloud removal

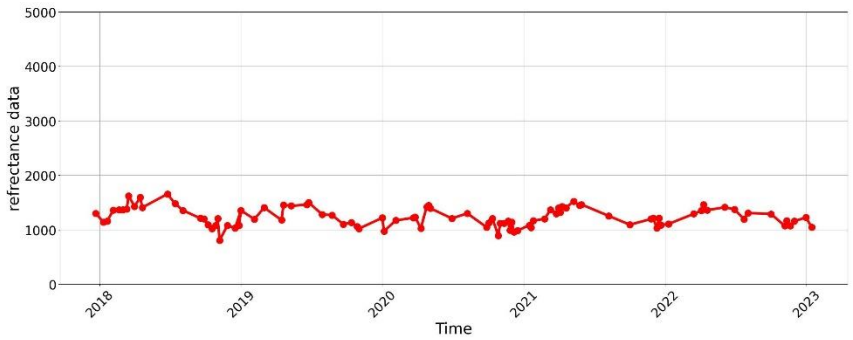

(b) After cloud removal

Figure 6: Comparison Before And After Cloud Removal.

In order to confirm that the clouds were removed at all periods, an image was created for each pixel in which the maximum reflectance was calculated for all periods (Figure 7).

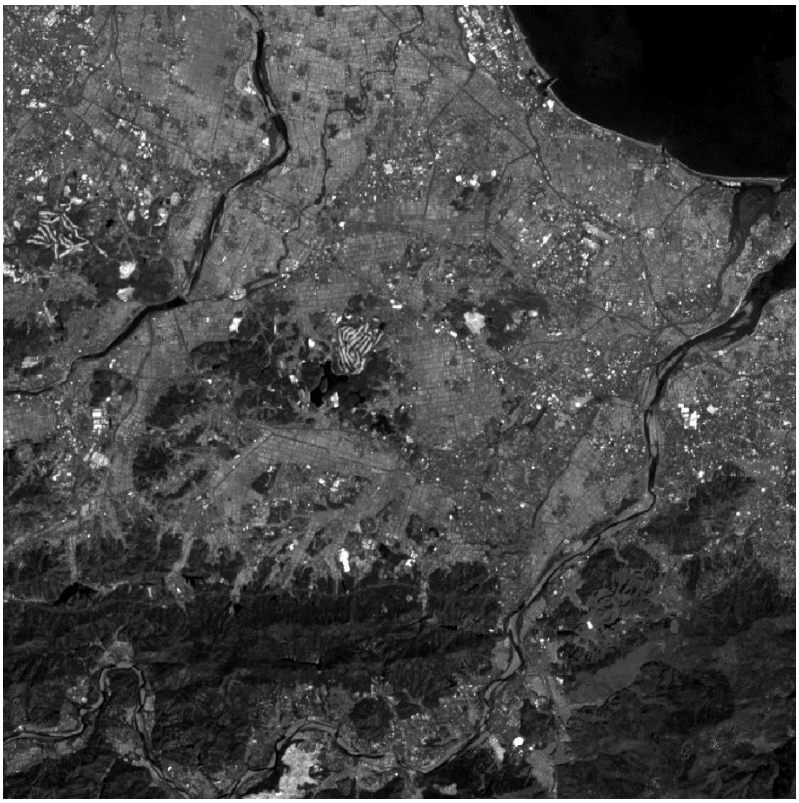

Figure 7: Maximum value composite of band 5 reflectance for the entire study period.

The absence of clouds in most pixels indicates that cloud removal is working well.

b. Detection of land cover change

Figure 8 shows the detected land cover change based on the change indicators in band 5 reflectance. Visual inspection was able to detect large size of changes by buildings and changes from forest to solar panels.

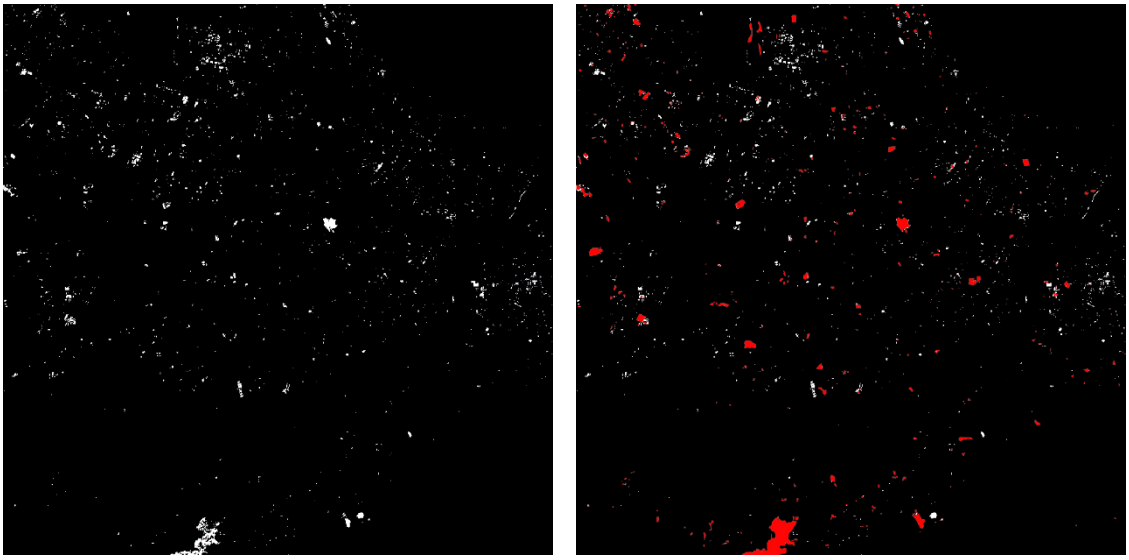

(a) Change detection (b) Overlay with validation data

Figure 8: Detection Results Of Land Cover Change At Band5.

An example of successful change detection is shown in Figure 9. Solar panels were constructed here between August 2018 and November 2018. In this example, the change in land cover resulted in a decrease in reflectance and successful detection.

(a) Before change (b) After change (c) Change detection

Figure 9: Successful Detection Example 1.

Another example of successful change detection is shown in Figure 10. This location was changed from agricultural field to a white roofed building in February of 2019. The change to a white roof is easy to detect because of the large change in reflectance.

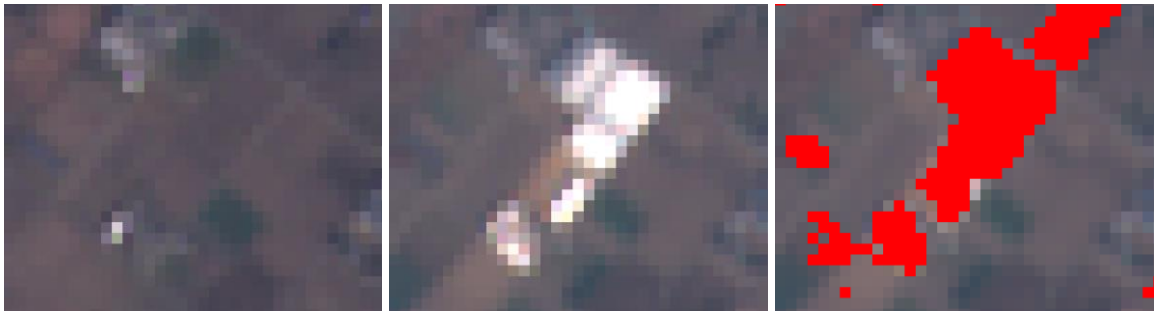

(a) Before change (b) After change (c) Change detection

Figure 10: Successful Detection Example 2.

However, there are many false positive pixels. There are two main reasons of false positives. First, the agricultural fields have been used for different crops from year to year, resulting in larger values in the change indicators since it compared the reflectance in two consecutive years. Figure 11 shows an example of a time series of pixels with false detection of agricultural fields. This agricultural field had false positives because it grew one crop a year some years and two crops a year others. The second reason is that cloud shadows cause false positives by greatly reducing reflectance. Figure 12 shows an example of a time series of pixels that were falsely detected due to the cloud shadows in the second half of 2021. The pixel was more susceptible to the cloud shadow, if ground object has higher reflectance. Then, the pixel is likely resulted in the false positive error.

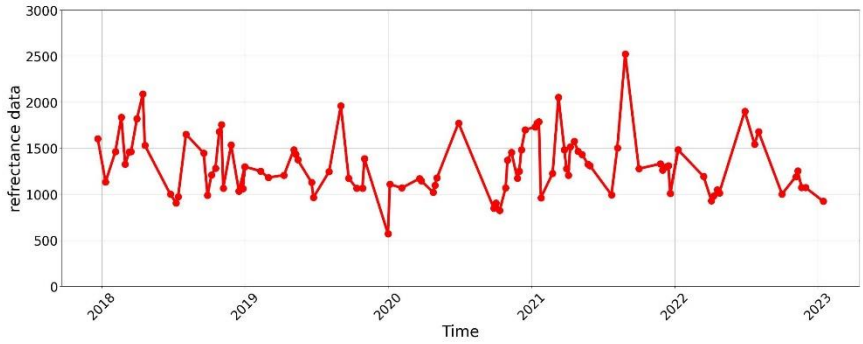

(a) Time series of reflectance

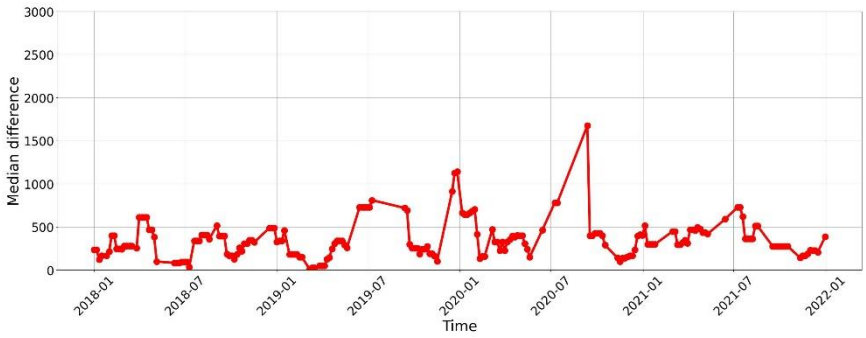

(b) Time series of change indicators

Figure 11: Time Series Of Band 8 Reflectance With False Detection Of Agricultural fields.

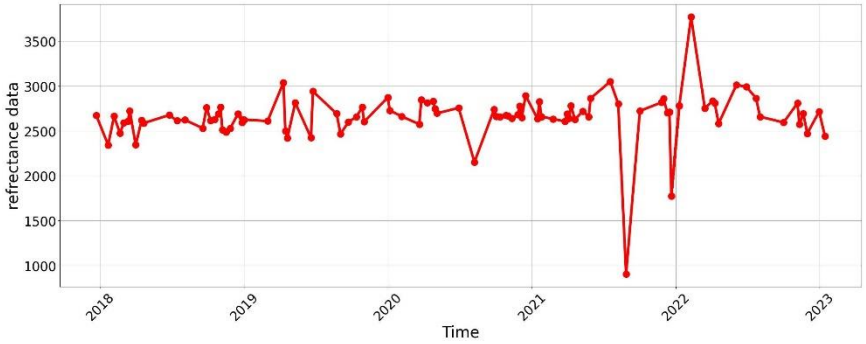

(a) Time series of reflectance

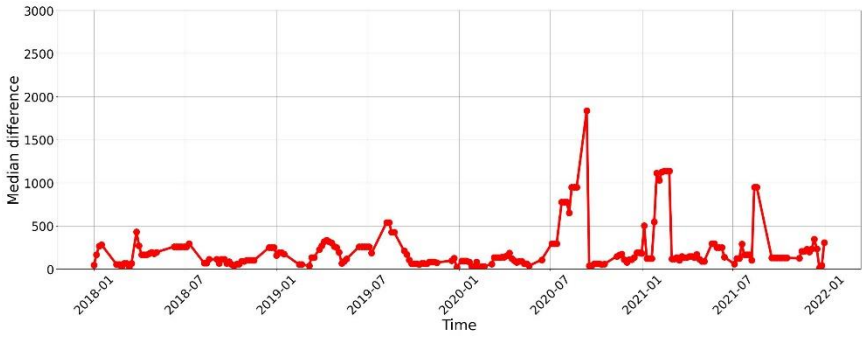

(b) Time series of change indicators

Figure 12: Time Series Of Pixels False Positives Due To Cloud Shadows.

c. Accuracy assessment by evaluation index

For quantitative evaluation, Precision, Recall, and F-measure were calculated. In evaluation case 1, 7094 manually selected changed pixels and 7403 randomly selected unchanged pixels were used. In evaluation case 2, the entire image (746496 pixels) except the validation pixels for the changed area was used. The results are shown in Table 4.

Table 4: Evaluation.

	Case 1			Case 2		
	F-measure	**Recall**	**Precision**	**F-measure**	**Recall**	**Precision**
Band 4	0.5733	0.4057	0.9769	0.3612	0.4057	0.3256
Band 5	0.5083	0.3435	0.9771	0.3358	0.3435	0.3285
Band 8	0.5463	0.4642	0.6637	0.0395	0.4642	0.0206
Band 11	0.5647	0.4180	0.8700	0.1071	0.4180	0.6145
Combined	0.7048	0.6795	0.7320	0.0526	0.6795	0.0273

Evaluation case 1 shows that there are few false positives, but there are many false negatives. For evaluation case 2, false positives are also frequent. If we could reduce the number of false positives in the entire image, so we aim to improve the accuracy in case 2. Bands 4, 5, and 11 had similar accuracy, but band 8 had more false positives and was less accurate than the other bands. The detection results for band 8 are shown in Figure 13. False positives of agricultural fields were much more common in band 8 than in the other bands. This did not change when the threshold was set to the same value as in the other bands.

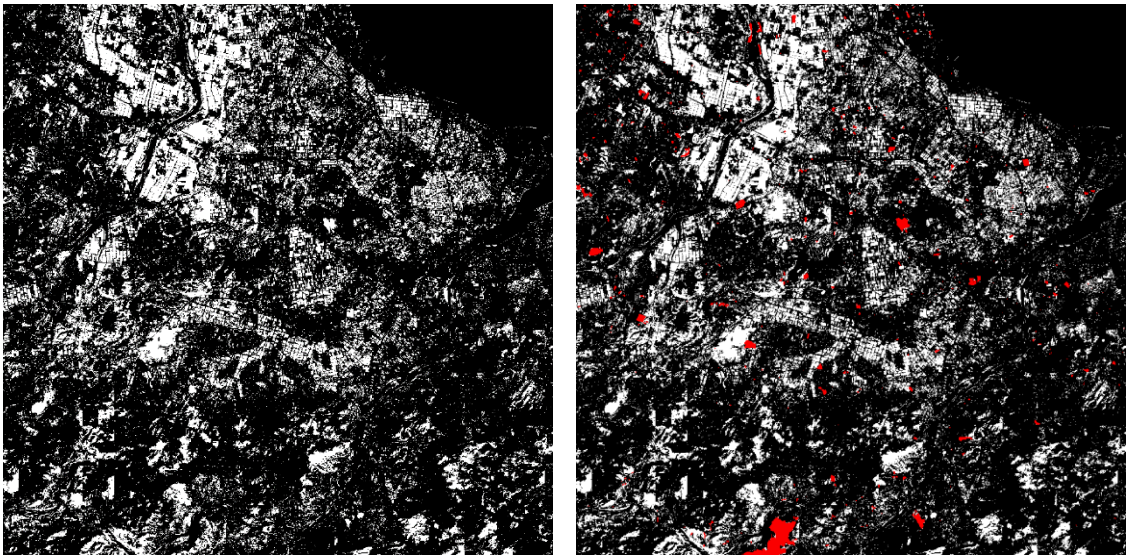

(a) Change detection (b) Overlay with validation data

Figure 13: Detection Results Of Land Cover Change At Band 8.

Band 8 (NIR) is more sensitive to vegetation and detects vegetation changes more easily. This resulted in more false positives and lower overall accuracy. The combined detection

was performed so that the pixel is considered as a change if any one of the four bands detects the change. The overall accuracy in case 1 was the highest at 0.7048, while in case 2, the overall accuracy was lower due to false positives in band 8. By changing the combination of bands and the conditions for change detection, the accuracy in case 2 can be higher than that of a single band. We also consider that if vegetation changes can be removed, the problem in band 8 can be solved and accuracy will be greatly improved.

d. The result of applying BFAST to this data

The BFAST (Verbesselt et al. 2010) was applied to this target area. As a result, it was not possible to detect land cover change well due to many false positives and negatives. There are two main reasons why it did not work. The first reason is the insufficient data length for fitting, as our target period was from 2019 to 2022. BFAST creates a time series model by fitting and detects changes from predicted and observed values. However, Sentinel-2 can only stably obtain data from 2018 onward, and there is still not enough data available. The second reason is that Japan has few clear days and many unavailable data. This is also a major problem in the fitting process, making it impossible to create a successful time series model. These two issues can be a problem with other fitting methods as well. Therefore, the current method is used instead of fitting.

Conclusion and Recommendations

a. Conclusion

In this study, a cloud mask created from Himawari was applied to Sentinel-2 for more accurate land cover change detection. As a result, most clouds were successfully removed by the cloud mask. By excluding most of the clouds, false positives due to clouds were greatly reduced. Many changes such as the construction of solar panel and building were successfully detected. The overall accuracy of land cover change detection with Band 5 alone was 0.34. There were many false positives due to agricultural fields and cloud shadows. We obtained similar results for bands 4, 5, and 11; however, the result for band 8 was different due to the influence of the vegetation. When combined with the other bands, Precision went down, but Recall increased to about 0.68. We consider that better results can be obtained by changing the way the bands are combined and the conditions of detection.

b. Recommendations

Because there are many false positives due to agricultural operations and cloud shadows, each of them should be improved in a different way. False positives due to agricultural operations are excluded from changes in vegetation-oriented changes using the Normalized Difference Vegetation Index (NDVI). We consider that if vegetation-oriented changes could be completely eliminated, the threshold for change detection could be relaxed and missed changes could be improved. On the other hand, the cloud shadow problem can be reduced resolved improved by creating cloud shadow masks from Himawari by more accurately estimating cloud heights.

In addition, four bands were used this time by selecting one band from each wavelength band such as red and NIR. However, we consider that more land cover changes can be detected by combining the detection results of all bands with a spatial resolution of 20 m or less.

In terms of evaluation, we will evaluate the time of the change in addition to the current evaluation of the location. Specifically, we consider evaluating dozens of locations in the reference data where the actual time of change has been identified.

References

Chai, B., & Li, P. (2023). An ensemble method for monitoring land cover changes in urban areas using dense Landsat time series data. Vol. 195. *ISPRS Journal of Photogrammetry and Remote Sensing*. Elsevier. https://doi.org/10.1016/j.isprsjprs.2022.11.002

Coluzzi, R., Imbrenda, V., Lanfredi, M., & Simoniello, T. (2018). A first assessment of the Sentinel-2 Level 1-C cloud mask product to support informed surface analyses. Vol. 217. *Remote Sensing of Environment*. Elsevier. https://doi.org/10.1016/j.rse.2018.08.009

Copernicus, Copernicus Open Access Hub, Retrieved September 9, 2024, from https://scihub.copernicus.eu/

Matsuoka, M., Honda, R., Nonomura, A., Moriya, H., Akatsuka, S., Yoshida, H., Takagi, H. (2016). A Method for Improving Geometric Accuracy of Himawari-8 “Japan Area” Data: Vol. 54. *Journal of the Japan Society of Photogrammetry and Remote Sensing*. J-STAGE. https://doi.org/10.4287/jsprs.54.280

Matsuoka, M., Yoshioka, H. (2023). Orthorectification of Data from the AHI Aboard the Himawari-8 Geostationary Satellite: Vol. 15. *Remote Sensing*. Multidisciplinary Digital Publishing Institute. https://doi.org/10.3390/rs15092403

Ministry of Land, Infrastructure, Transport and Tourism. Satellite Remote Sensing Data Application Task Force Ministerial Meeting Materials. Retrieved September 8, 2024, from https://www8.cao.go.jp/space/taskforce/rs/dai3/siryou1_3_1.pdf

QGIS. Retrieved September 12, 2024. from https://qgis.org/

Sentinel Online. Spectral Resolutions of Sentinel-2. Retrieved September 8, 2024. from https://sentinel.esa.int/en/web/sentinel/user-guides/sentinel-2-msi/resolutions/spectral

SentiWiki. Sentinel-2. Retrieved September 11, 2024, from https://sentiwiki.copernicus.eu/web/s2-processing

Verbesselt, J., Hyndman, R., Zeileis, A., & Culvenor, D. (2010). Phenological change detection while accounting for abrupt and gradual trends in satellite image time series: Vol. 114. *Remote Sensing of Environment*. Elsevier. https://doi.org/10.1016/j.rse.2010.08.003

Verbesselt, J., Zeileis, A., & Herold, M. (2012). Near real-time disturbance detection using satellite image time series. Vol. 123. *Remote Sensing of Environment*. Elsevier. https://doi.org/10.1016/j.rse.2012.02.022

Wright, N., Duncan, J. M. A., Callow, J. N., Thompson, S. E., & George, R. J. (2024). CloudS2Mask: A novel deep learning approach for improved cloud and cloud shadow masking in Sentinel-2 imagery: Vol. 306. *Remote Sensing of Environment*. Elsevier. https://doi.org/10.1016/j.rse.2024.114122

Zhu, Z., & Woodcock, C. E. (2014). Continuous change detection and classification of land cover using all available Landsat data: Vol. 144. *Remote Sensing of Environment.* Elsevier. https://doi.org/10.1016/j.rse.2014.01.011